

**Lead and antimony in basal ice from Col du Dome (French Alps) dated with radiocarbon:  
A record of pollution during Antiquity**

Susanne Preunkert<sup>1</sup>, Joseph R. McConnell<sup>2</sup>, Helene Hoffmann<sup>3,4</sup>, Michel Legrand<sup>1</sup>, Andrew Wilson<sup>5</sup>, Sabine Eckhardt<sup>6</sup>, Andreas Stohl<sup>6</sup>, Nathan Chellman<sup>2</sup>, Monica Arienzo<sup>2</sup>, Ronny Friedrich<sup>7</sup>

<sup>1</sup>Université Grenoble Alpes, CNRS, Institut des Géosciences de l'Environnement (IGE), Grenoble, France

<sup>2</sup>Division of Hydrologic Sciences, Desert Research Institute, Reno, Nevada, USA

<sup>3</sup>Institute of Environmental Physics, Heidelberg University, Heidelberg, Germany

<sup>4</sup>Alfred-Wegener-Institut Helmholtz Zentrum für Polar- und Meeresforschung, Bremerhaven, Germany

<sup>5</sup>Faculty of Classics, University of Oxford, Oxford, United Kingdom

<sup>6</sup>Department of Atmospheric and Climate Research, Norwegian Institute for Air Research, Kjeller, Norway

<sup>7</sup>Curt-Engelhorn-Center Archaeometry, Mannheim, Germany

**Contents of this file**

Text S1 to S4

Figures S1 to S3

Tables S1 to S2

**Additional Supporting Information (Files uploaded separately)**

Supporting data are included as Dataset S1 and S2. The SI file Preunkert-ds01.xlsx contains the CDD Pb and Sb records over depth and age as reported in Figure 2. The SI file Preunkert-ds02.xlsx contains FLEXPART-simulated lead emissions sensitivities for the CDD and NGRIP2 (McConnell et al., 2018) as reported in Figure 3.

## Introduction

The supporting information contains: the calculation of enrichment factors and non-crustal contributions using Ce data (Text S1); an explanation of the CDK basal ice dating (Text S2); a comparison of the CDK lead and antimony ice concentrations with previous alpine ice studies (Text S3); and the use of the FLEXPART atmospheric aerosol transport and deposition model (Text 4). In Figure S1 we compare the CDK lead record with the Lake sediment lead record from Meidsee (Switzerland) (Thevenon et al., 2011) as well as with lead records from three European peat bogs (Bindler et al., 1999; Le Roux et al., 2004; Martinez Cortizas et al. 2002), while in Figure S2 the CDK lead record is compared to those available from CG. In Figure S3 we report calculated enrichment factors and non-crustal contributions of lead and antimony in CDK. In Table S1 we give an overview of masses and  $^{14}\text{C}$  ages of the CDK ice core samples, and in Table S2 we summarize lead and antimony ice concentrations of Alpine ice cores over various time periods.

### Text S1.

Crustal lead was subtracted from measured total lead to yield non-crustal lead that included both the volcanic and pollution components. Lead enrichment factor (Figure S3) was calculated as the ratio of lead to cerium measured in ice samples divided by the ratio for mean sediment (0.23, Bowen, 1966). An  $\text{EF}_{\text{Ce}}$  value equal to unity indicates that all lead present in the ice can be attributed to continental dust. As seen in Figure S3, the  $\text{Pb-EF}_{\text{Ce}}$  reached a minimum of 3 at the beginning of classical antiquity and in late antiquity at CDD when a minimum of Pb concentrations is observed ( $0.015 \text{ ng g}^{-1}$ , Figure 2b).

Whereas the crustal Pb (cPb) contribution remains very weak compared to the total (18 % on average from 1000 BCE to 500 CE), the use of the mean sediment Sb/Ce ratio (0.0144) leads to several negative values of the ncSb fraction and Sb- $\text{EF}_{\text{Ce}}$  values lower than unity (see Figure S3). Assuming, as an upper limit, that the minimum of the Sb/Ce ratio seen at 500 CE (0.085, Figure S3f) corresponds to the terrestrial fraction of Sb reaching the CDD site, we calculated a Sb/Ce ratio of 0.005 (instead of 0.0144 in mean sediments, Bowen, 1966), and used this value to calculate the non-crustal Sb contribution reported in Figure 2.

### Text S2.

As reported in Table S1,  $^{14}\text{C}$  data suggest that the CDK ice core extends back to  $\sim 5000 \pm 600$  cal yr BP. A non-linear depth-age relationship is observed in the CDK basal ice (Figure 1), as typically seen in high Alpine glaciers frozen to bedrock like CG (Lüthi & Funk, 2000) and CDD (Gilbert et al., 2014). Considering this typical non-linear age-depth characteristic, a two-parameter fit (based on a simple analytical expression for the decrease of the annual layer thickness with depth) was used to interpolate the ages of the lowermost four  $^{14}\text{C}$  samples to a continuous age-depth relation (Nye, 1963; Jenk et al., 2009). From that, the age (T in yr) can be derived as function of depth (z in mwe):

$$T(z) = \frac{H}{b \cdot p} \left( \left( 1 - \frac{z}{H} \right)^{-p} - 1 \right) \quad \text{Eq. 1}$$

where  $H$  is the ice thickness (here 95.65 mwe),  $b$  is the annual accumulation rate in mwe, and  $p$  the thinning parameter (dimensionless), under border condition  $T(0) = 0$ . Iterative curve fitting on the basis of Newton's method for estimating the parameters was used to fit the four  $^{14}\text{C}$  dates by varying  $b$  and  $p$ . The result for the four  $^{14}\text{C}$  dates (without considering their uncertainties) and  $H = 95.65$  mwe (taken as the total ice core length) was  $b = 2.0$  mwe and  $p = 0.80$  with a fit error of 220 yrs.  $b$  is in good accordance with what is expected, and  $p$  is very close to what was found at CG by Jenk et al. (2009) ( $0.87 \pm 0.05$ ). However, intended only to serve for the interpolation of data, the fit has substantial limitations and caution should be used in how it is interpreted since: (1) fitting was not applied over the whole core and  $^{14}\text{C}$  date uncertainties were not considered; (2) the parameterization is very sensitive to the absolute glacier thickness and different from real conditions; and (3) the applied function assumes temporal and upstream constant accumulation rate which certainly is not true for the CDK drill site.

### **Text S3.**

Table S2 summarizes and compares lead and antimony concentrations from this work on the CDD ice (CDK, C10, C11 cores) with those previously obtained in alpine ice. We compared concentrations measured during different time periods including before and after large anthropogenic emissions began in the 20th century. Details on the dating of the C10 ice core can be found in Legrand et al. (2018).

Table S2 shows that the new measurements are in excellent agreement for all lead studies of the modern ice with levels being on average close to  $2\text{--}3 \text{ ng g}^{-1}$ . The same is true (within a factor of two) for Sb with a consistent mean value close to  $0.020$  to  $0.050 \text{ ng g}^{-1}$ . All data for ice deposited during the 19th century indicate a drop of lead concentration towards  $\sim 0.75 \text{ ng g}^{-1}$  with respect to those observed during the 20th century. All data from the 18th century also consistently indicate a decrease of Sb to  $0.008 \text{ ng g}^{-1}$  with respect to the 20th-century values. Finally, whereas all lead data from periods before the 19th century indicate values close or lower than  $0.3 \text{ ng g}^{-1}$ , dating uncertainties of the different ice cores, as well as differences in analytical approaches and different temporal resolution of the CDD (e.g., 16 cm we from 400 to 600 CE) and CG (e.g., 67 cm we from 500 to 700 CE in the record of Gabrieli & Barbante (2014)) render comparisons difficult in the older alpine ice layers. However, note that all three studies report minimum values close to  $0.040 \text{ ng g}^{-1}$  prior to the Middle Ages, whereas maximum values are far higher at CG compared to CDD during this period. In particular, as shown in Figure S2b, the CG lead profile from More et al. (2017) exhibits numerous sudden increases of lead concentrations (well above  $1 \text{ ppb}$ ) that were not attributed to specific events. Note that, (1) these spikes cannot be explained by a higher time resolution of the CG record compared to the CDK record (see caption of Figure S2), and (2) no peak is observed in peat bog records (Figure S1) between the end of the Roman period and the beginning of the Middle Ages.

### **Text S4.**

To identify and evaluate possible provenance of lead deposited at the CDD site, we used the well-established Lagrangian particle dispersion model FLEXPART (Stohl et al., 2005). We took advantage of a new development that allows running the model backward in time for dry and wet deposition quantities (Eckhardt et al., 2017). As with the more typical backward calculations for atmospheric concentrations (Seibert and Frank, 2004), the output of the model

calculations is a source-receptor relationship that maps sensitivity of the modelled deposition at the selected measurement (receptor) site (i.e., the CDD ice-core site) to an emission (source) flux (i.e., mining and smelting sites during antiquity). With a prescribed atmospheric emission field, lead sources and deposition can be calculated by multiplying the model output by the emission flux.

Following McConnell et al. (2018), the model was run in backward mode from both CDD and NGRIP2 locations at monthly intervals for the period 1920 through 1999, and particles were traced backward for 30 days corresponding to several times the average lifetime of the tracked aerosol. Lacking the detailed meteorological fields necessary for modelling lead transport in ancient times, we used the recently completed coupled climate reanalysis for the 20<sup>th</sup> century (CERA-20C) (Laloyaux et al., 2017) performed at the European Centre for Medium Range Weather Forecasts (ECMWF) and assumed that average atmospheric transport patterns during this recent period were representative of those during antiquity. Lead aerosols were modelled with an assumed logarithmic mean diameter of 1.0  $\mu\text{m}$  (standard deviation of 0.9) and we used the reanalysis data at a resolution of 2° x 2° and every six hours.

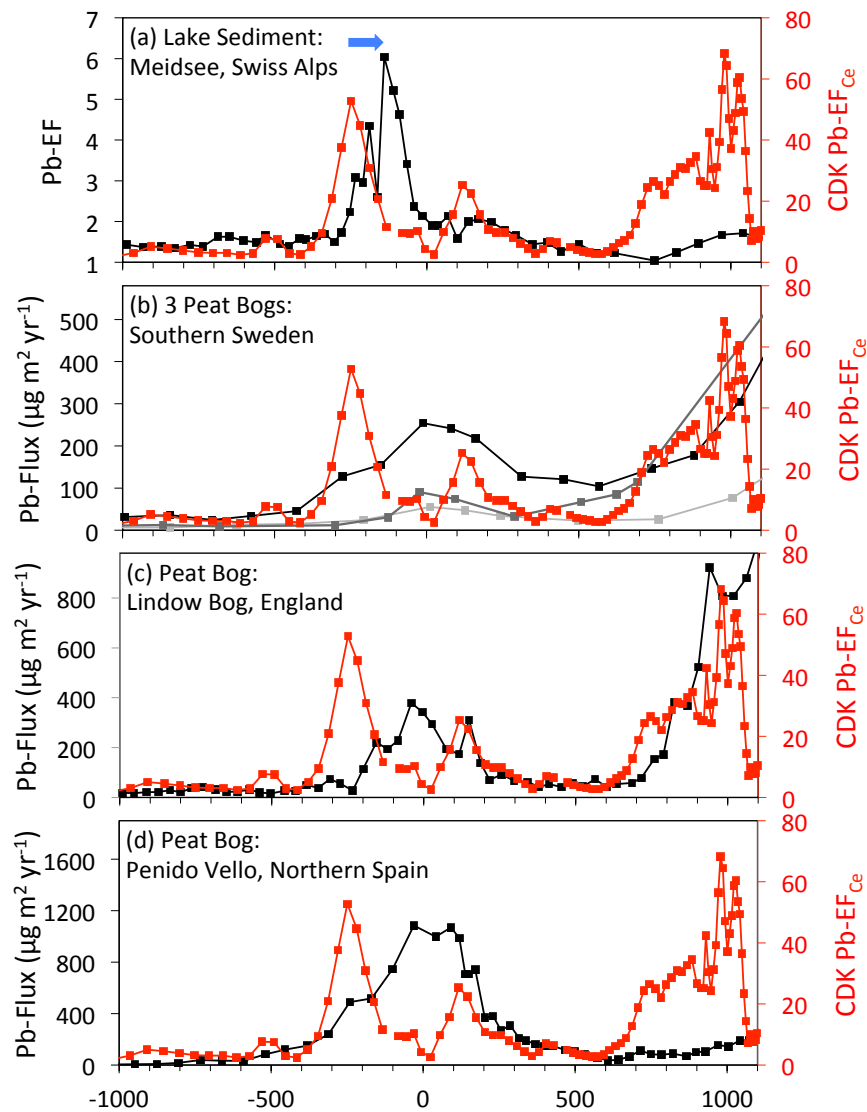


**Figure S1.** Comparison of Pb enrichment factors in CDK ice (red curve) with (a) a lake-sediment record from the alpine lake Meidsee, Switzerland (Thevenon et al., 2011, see also Bindler et al., 2018), located about 80 km from the CDD site, and (b-d) three European peat bog records from southern Sweden (Bindler et al., 1999), England (Le Roux et al., 2004, see also Bindler, 2018), and northern Spain (Martínez Cortizas et al., 2002, see also McConnell et al., 2018). Note that the lead perturbation assigned to ~250 BCE in CDK is potentially some 110 years too old as denoted by the blue arrow (see section 3). This Republican period peak seen in both the CDD and the Meidsee record, but not in the records from Sweden, England, or northern Spain, appears to represent pollution from mining sources relatively close to the Alps.

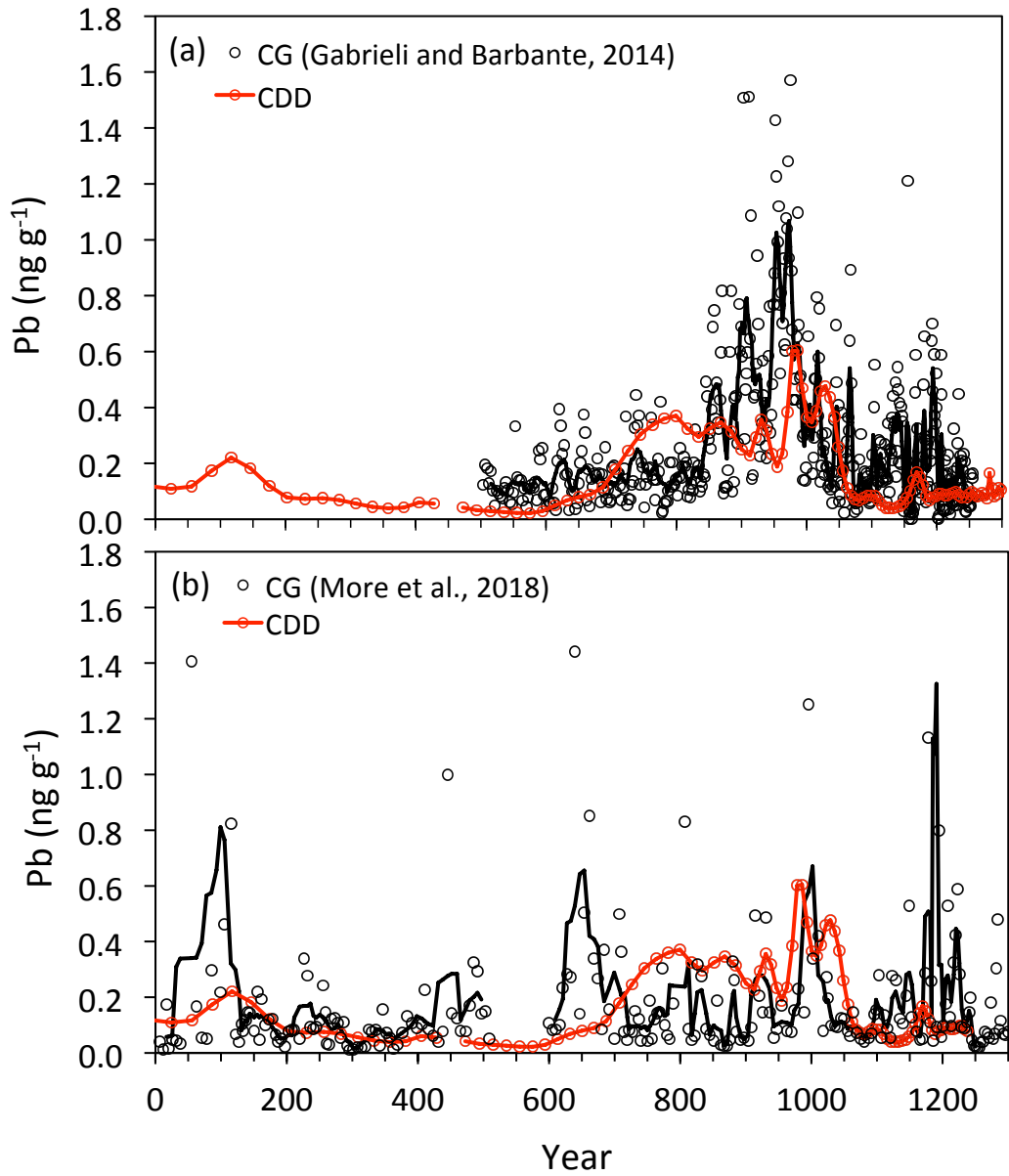


**Figure S2.** Comparison of Pb concentrations in CDK ice (red curve) with available lead records from CG ((a) Gabrieli & Barbante, 2014, and (b) More et al., 2017) over common time periods (see section 3). Black circles are raw data. The black lines correspond to running mean curves, for which the time window was chosen to obtain similar sampling resolutions than in CDK.

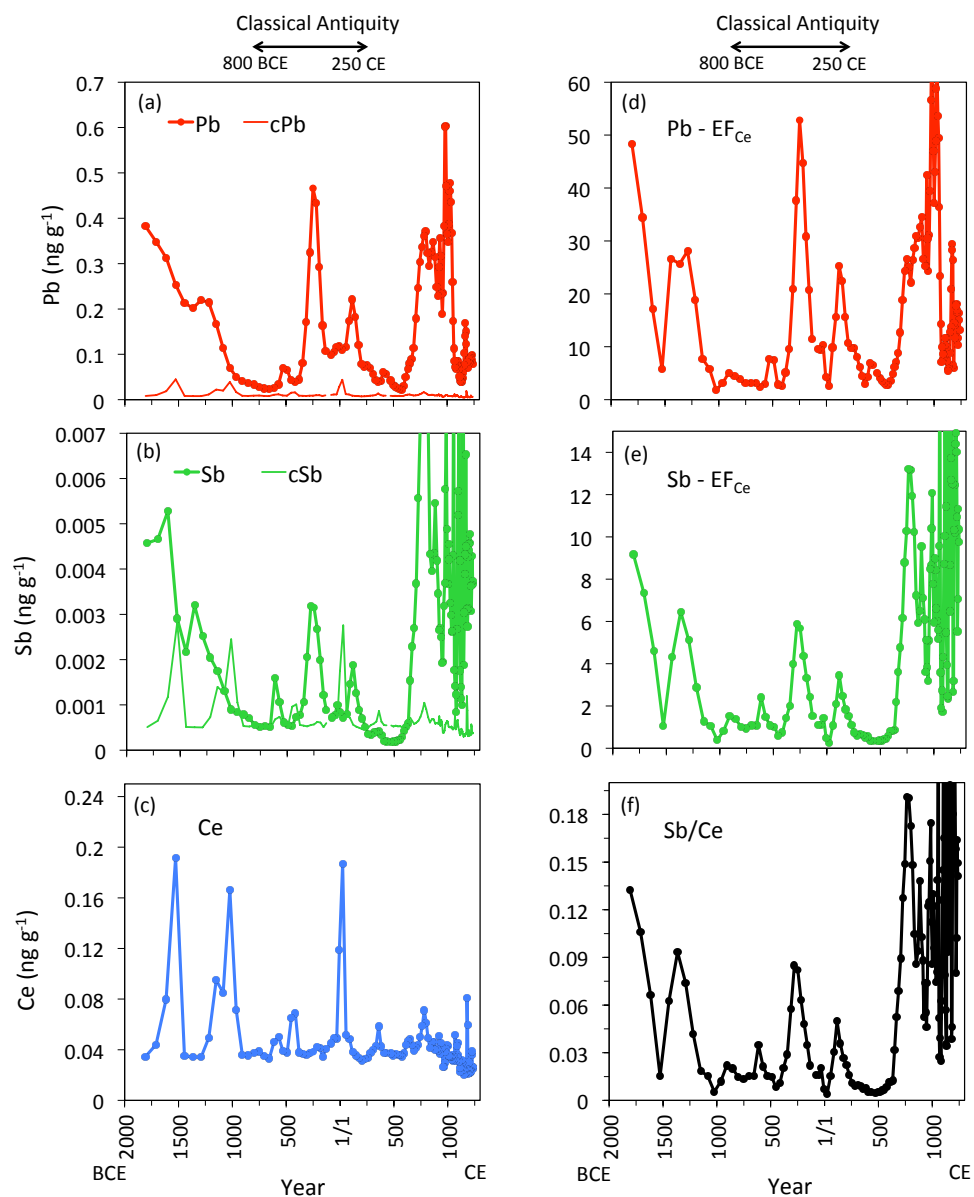


**Figure S3.** Left: Lead (a), antimony (b), and cerium (c) CDK records (thick lines and dots) in the basal ice. The crustal fractions of lead and antimony (cPb and cSb in a and b) are reported as thin lines. Right: Lead (d) and antimony (e) enrichment factors (Pb-EF<sub>Ce</sub> and Sb-EF<sub>Ce</sub>) with respect to cerium (see section 2) and Sb/Ce ratio (f) in basal CDK ice. The red dashed line in the Sb/Ce ratio (f) is the mean sediment value from Bowen (1966). Measured Ce concentrations were multiplied by 1.66 to account for under-recovery during the continuous measurements (see section 2.1).

Sample Name	Depth [mwe]	Mass [g]	POC mass corrected [ $\mu\text{gC}$ ]	$^{14}\text{C}$ corrected [ $\text{F}^{14}\text{C}$ ]	Calibrated $^{14}\text{C}$ date BCE/CE at 68.2%	Calibrated $^{14}\text{C}$ age range at 68.2% [yr cal BP]	Calibrated $^{14}\text{C}$ -age [yr cal BP] mean
CDK-173	90.53 - 90.95	360	2.6	$1.010 \pm 0.068$	1450 CE - Modern	500 - Modern	410
CDK-176	91.65 - 92.05	310	3.0	$0.820 \pm 0.064$	350 BCE - 1020 CE	2300 - 930	1710
CDK-178	92.65 - 93.09	460	2.8	$0.922 \pm 0.068$	780 CE - Modern	1170 - Modern	820
CDK-179	93.49 - 93.85	320	8.1	$0.829 \pm 0.041$	80 CE - 950 CE	1870 - 1000	1510
CDK-181/182	94.55 - 94.89	305	8.1	$0.759 \pm 0.026$	740 BCE - 50 CE	2690 - 1900	2250
CDK-183	95.15 - 95.39	215	5.1	$0.577 \pm 0.034$	3650 BCE - 2470 BCE	5600 - 4420	5020

**Table S1.** Overview of masses (corrected for blanks but not for combustion efficiency) and  $^{14}\text{C}$  ages of the CDK ice core samples combusted in the REFILOX system. Calibrated date ranges are shown at 68.2% probability and rounded according to Millard (2014).



Site	Time period		Pb (in ng g <sup>-1</sup> )	Sb (in ng g <sup>-1</sup> )	References
CG	Prior to the Middle Age	500-700 CE	0.293 ± 0.339 (0.05-1.44)	-	More et al. (2017)
CG		500-700 CE	0.137 ± 0.082 (0.03-0.39)	-	Gabrieli & Barbante (2014)
CDD <sup>a</sup>		400-600 CE	0.036 ± 0.014 (0.022-0.050)	0.0003 ± 0.0001	This work
CG	19 <sup>th</sup> century	1880-1900	0.7 ± 0.3	-	Schwikowski et al. (2004)
CG		1650-1900	-	0.008	Barbante et al. (2004)
CDD <sup>b</sup>		1850-1900	-	0.008 ± 0.005	Van de Velde et al. (1999)
CDD <sup>c</sup>		1890-1900	0.8 ± 0.2	0.009 ± 0.003	This work
CG	Modern	1970-1975	~3.0	-	Gabrieli & Barbante (2014)
CG		1960-1985	2.7 ± 0.3	-	Schwikowski et al. (2004)
CG		1900-2000		0.048	Barbante et al. (2004)
CDD <sup>b</sup>		1950-2000	-	0.021 ± 0.005	Van de Velde et al. (1999)
CDD <sup>c</sup>		1970-1980	2.3 ± 0.7	0.020 ± 0.006	This work

<sup>a</sup> denotes the CDK ice core, <sup>c</sup> the C10 ice core, and <sup>b</sup> the C11 ice core drilled a few meters from the C10 during the same field campaign.

**Table S2.** Summary of lead and antimony ice concentrations (mean ± standard deviation) obtained in this work and previous studies both for pre-industrial ice and modern ice. Pb values under parenthesis refer to minimum and maximum values.